

**Submonolayer iron film growth on reconstructed Ir(100)-(5×1)**

L. Hammer, W. Meier, A. Schmidt, and K. Heinz

*Lehrstuhl für Festkörperphysik, Universität Erlangen-Nürnberg, Staudtstrasse 7, D-91058 Erlangen, Germany*

(Received 31 October 2002; published 31 March 2003)

The early stages of iron film growth on the quasihexagonally reconstructed Ir(100)-(5×1) surface were investigated for deposition temperatures 90–450 K by means of scanning tunnelling microscopy and quantitative low-energy electron diffraction (LEED). For low coverage, single iron atoms diffuse within the one-dimensional troughs formed through the top layer reconstruction. On large step-free terraces a metastable iron phase develops consisting of linear diatomic Fe chains which reside within the troughs and are homogeneously spread over the terrace. With increasing coverage and controlled by temperature, the hexagonal reconstruction is lifted. This surface restructuring proceeds by expelling the 20% extra Ir atoms accommodated in the quasihexagonal layer, whereby a new (5×1) superstructure consisting of equally spaced Ir rows is formed at the very surface. With further deposition, iron fills the space between these rows, eventually leading to an ordered Fe<sub>4</sub>Ir surface alloy with the completion of the top layer. A quantitative LEED analysis corroborates this model and reveals significant atomic corrugations down to the third layer. It is observed that surface defects of any kind act as nucleation centers for both the film growth and the restructuring process.

DOI: 10.1103/PhysRevB.67.125422

PACS number(s): 61.14.-x, 68.35.Ct, 68.43.Fg, 68.55.Ac

**I. INTRODUCTION**

The heteroepitaxial growth of discrete thin magnetic films and of superlattices consisting of magnetic layers and non-magnetic spacers is a highly interesting and a rapidly growing field of research. Due to the reduced dimensionality and the epitaxial substrate imposed strain, the crystallographic and magnetic structure of the growing film is expected to deviate from bulk properties opening a wide field for tailoring magnetic devices. The system Fe/Ir(100) seems to be a promising candidate in this sense from a number of reasons: The magnetic characteristics of iron depend crucially on both the crystallographic structure and the atomic volume<sup>1,2</sup> and so will heavily be influenced by pseudomorphic growth as reported earlier.<sup>3–5</sup> Second, the atomic nearest neighbor distance within an Ir(100) plane (2.72 Å) falls just between the corresponding values of fcc and bcc Fe(100) (2.56 and 2.87 Å, respectively). Consistently, a new body-centered tetragonal (bct) Fe phase with a *c/a* ratio of about 1.25 has been found in FeIr superlattices.<sup>3,5</sup> The magnetic properties of these superlattices have been subject to recent research (e.g., Refs. 6–10). Finally, layer-by-layer growth has been observed for thin Fe films on Ir(100) with a sharp interface to the substrate.<sup>3</sup> Since the growth of Ir on the Fe films is also two dimensional,<sup>4</sup> high-quality superlattices can be prepared as model systems for various investigations.

However, from the physics point of view the above described growth mode appears surprising. The stable phase of (clean) Ir(100) is reconstructed with the top atomic layer exhibiting (5×1) periodicity due to an almost hexagonally close-packed atomic arrangement.<sup>11,12</sup> Its accommodation to the underlying quadratic substrate involves a vertical buckling of atoms within the hexagonal layer whereby a maximum amplitude of about 0.5 Å was determined by quantitative low energy electron diffraction (LEED) (Refs. 13–16) and scanning tunnelling microscopy (STM).<sup>17</sup> So, pseudomorphic growth on a reconstructed Ir(100) surface should not lead to a bct structured Fe film. On the other hand, the lifting of the reconstruction under the influence of small

amounts of deposited iron has been observed for the similarly reconstructed Au(100) surface (e.g., Refs. 18,19). If this would also take place for Ir(100), substantial atomic intermixing at the interface must be expected, since 1/5 of Ir atoms have to be expelled from the top layer upon this restructuring. So, atomically flat interfaces as observed in the FeIr superlattices<sup>5</sup> cannot be chemically homogeneous.

Therefore, the present study is devoted to the initial steps of film growth in the submonolayer regime. A combination of STM and quantitative LEED investigations give access to morphological and crystallographic information. After a short description of the experimental and computational procedure we will demonstrate that Fe first nucleates as metastable bi-atomic chains on top of the reconstructed Ir(100) surface, the reconstruction is lifted with increasing coverage (and temperature) in a thermally activated process, and an ordered surface alloy is eventually formed for coverages in the monolayer regime.

**II. EXPERIMENTAL AND COMPUTATIONAL**

The experimental equipment was accommodated in a two-chamber apparatus (pressure  $<5 \times 10^{-11}$  mbar during experiment). One chamber hosted a commercial variable temperature STM (beetle design, RHK). In the present study it was operated at room temperature since, for the transfer from the preparation chamber, the samples had to be brought to ambient temperatures after preparation. The other vessel contained a home-made retractable three-grid rear-view LEED optics and a hemispherical electron analyzer with separate 5 keV electron gun and dual-anode x-ray source for Auger electron spectroscopy (AES) and x-ray photoelectron spectroscopy (XPS) to check for sample cleanliness. Highly purified Fe was supplied by an electron beam evaporator (0.3 ML/min, pressure increase during operation  $<2 \times 10^{-11}$  mbar). The sample temperature was measured by means of a directly attached NiCr-Ni thermocouple. Sample heating up to about 1600 K was accomplished via electron bombard-

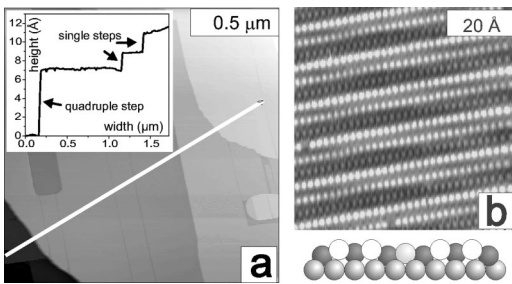


FIG. 1. STM images of Ir(100)-(5 $\times$ 1). (a) Large scale image (1.5 $\times$ 1.5  $\mu$ m) and height profile along the line displayed. (b) Atomically resolved images with every second locally protruding row visible as indicated below (85 $\times$ 85  $\text{\AA}$ ).

ment from the rear whilst cooling was achieved by direct contact to a liquid nitrogen reservoir.

The spark eroded and polished sample (surface roughness  $< 0.03 \mu\text{m}$ , alignment accuracy  $\leq 0.1^\circ$ ) was *in situ* prepared by initial sputtering (2 keV Ar $^+$ , 30  $\mu\text{A}/\text{cm}^2$ , 5min) followed by cycles of oxygen annealing ( $2 \times 10^{-7}$  mbar O $_2$ , 1300 K, 2min) and final flashes to 1400–1500 K. After this, no contaminations could be detected by AES/XPS and this state could be maintained by repeating the mentioned annealing in oxygen typically once a day. Deposited Fe films were sputtered off to avoid gradual bulk alloy formation. The clean surface exhibited atomically flat terraces of up to micrometer size often separated by 10–20  $\text{\AA}$  high steps [Fig. 1(a)]. All terraces were reconstructed with large domains of the two orthogonal orientations. Often, only one orientation was present on a terrace. The (5 $\times$ 1) reconstruction was usually imaged in STM by a typical pin stripe pattern. Under favorable tip conditions every second (protruding) atomic row could be resolved [Fig. 1(b)]. Consistent with the STM images, a clear and low background two-domain (5 $\times$ 1) LEED pattern was observed with sharp superstructure spots which were visible up to 1000 eV due to the high Debye temperature of Ir [430 K (Ref. 20)].

The STM images shown were recorded with negative tip voltages at about 0.5 V and 2 mV for large scale and atomically resolved images, respectively. As usual for metal surfaces, there was no strong dependence of the image contrast on voltage. For the intensity measurements entire LEED patterns taken at normal incidence and with the sample at about 90 K were recorded in steps of 0.5 eV in the energy range 50–600 eV by means of a 12-bit digital CCD camera. At each energy eight images were averaged and stored on a computer's hard disk taking about 15 min in total. Beam intensities by off-line evaluation resulted from a pixelwise and background corrected summation within a square frame around each spot. Intensity vs energy spectra  $I(E)$  of symmetrically equivalent spots were averaged, slightly smoothed whenever necessary, and finally normalized to the energy dependent primary beam intensity.

The calculation of LEED intensities was performed using the TensErLEED program package,<sup>21</sup> which provides the tensor LEED perturbation method<sup>22,23</sup> to consider geometrical, chemical,<sup>24,25</sup> and vibrational<sup>26</sup> surface properties. Up to

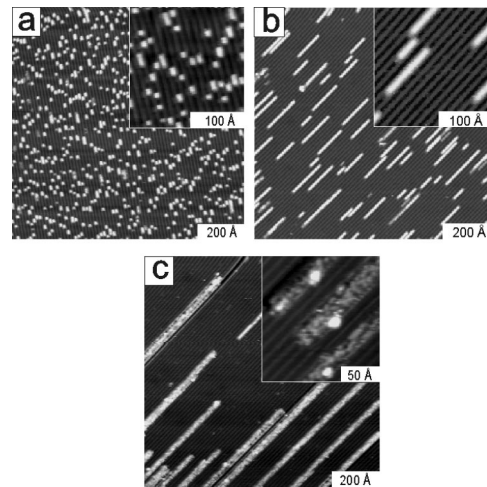


FIG. 2. STM images of a 0.07 ML Fe film deposited on Ir(100)-(5 $\times$ 1) with the sample at (a) 90, (b) 300, and (c) 450 K. In the insets the alignment of the Fe chains with respect to the troughs of the surface reconstruction is visible.

14 relativistically calculated and spin averaged phase shifts were used and electron attenuation was described by a constant imaginary part of the inner potential  $V_{0i}$ . The real part  $V_{0r}$  was allowed to be energy dependent as calculated via a program package provided by Rundgren.<sup>27</sup> Possible vacancies within the Fe layer were considered using the average  $t$ -matrix approximation (ATA).<sup>28,29</sup> The structural search was made by a frustrated simulated annealing procedure<sup>30</sup> guided by the Pendry  $R$ -factor  $R_p$ .<sup>31</sup> The latter was also applied to quantify the best-fit and to compare different experimental spectra. Its variance  $\text{var}(R_p)$  was used to estimate statistical errors of the analysis, whereby possible parameter correlations were neglected as usual.

### III. NUCLEATION OF IRON ON RECONSTRUCTED Ir(100)-(5 $\times$ 1)

For the initial growth regime the adsorption site and the mechanism of island nucleation are relevant. It is also essential to investigate the reconstruction's role for surface diffusion and its stability under adsorption. At low coverage, LEED is usually rather insensitive with respect to the presence of nonordered adatoms. Indeed, up to about 1/4 monolayer (ML) Fe coverage [1 ML corresponds to 1 adatom per Ir atom of a (100) Ir layer], the (5 $\times$ 1) LEED pattern hardly changes and there are no considerable modifications in the  $I(E)$  spectra (see Sec. IV). Therefore, we investigated the initial stages of Fe film growth exclusively by means of STM.

#### A. Formation of chainlike islands

Figure 2(b) displays a 0.07 ML Fe film deposited at room temperature, as it develops on a large reconstructed terrace. There are numerous chainlike islands all of the same height and homogeneously distributed over the surface. As visible in the inset, the chains are all aligned along the [011] direction (i.e., the direction of the surface reconstruction stripes)

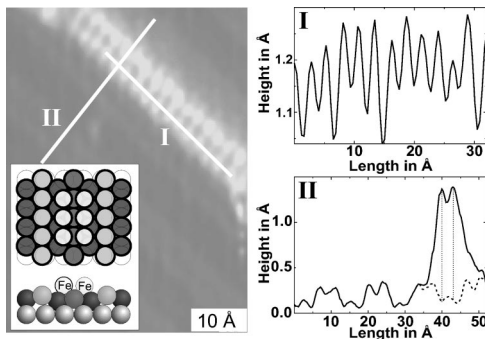


FIG. 3. Left: Atomically resolved STM image of a single Fe double chain on Ir(100)-(5 $\times$ 1)(50 $\times$ 70 Å). In the schematic model (inset) white balls correspond to the dual-row Fe chain. Right: The profiles in panel (b) are taken along the lines given in the STM image.

and located right above the troughs of the corrugated surface. Their apparent height above the trough bottom varies around 2 Å depending on the tunnelling conditions. Note that the islands never coalesce, even when neighbored in adjacent troughs. The reconstruction pattern is undisturbed in the immediate surroundings of the chains indicative for the reconstruction's persistence also below the islands. When Fe is deposited with the sample at 90 K, again chainlike islands develop. Yet, they now are more numerous and shorter [see Fig. 2(a)]. On the other hand, the chain length is increased for deposition at higher temperatures due to the increased diffusion length [see Fig. 2(c)]. The chains can extend to many thousand Å. Additionally, most of the reconstruction troughs remain unoccupied, indicating that—as Fe was evenly deposited at the surface—there now is a finite probability for diffusion across the “hills” of the reconstruction. Accordingly, Fig. 2(c) reveals that the chains have also gained in width. They are no longer confined to the bottom of the reconstruction troughs as in case of lower adsorption temperatures, but extend over two or three rows of the reconstruction. Also, their height appears rather inhomogeneous in STM. Thus, these islands must own a structure much different from that observed for lower temperatures. They develop only by overcoming a significant activation barrier. Equivalently, the phase of small Fe chains must be metastable, consistent with the fact that the conversion to broader islands takes also place when room temperature deposited films are annealed at 450 K. Section IV will show that this new island type is connected with a local lifting of the surface reconstruction.

### B. Structure of chainlike islands

As the STM appearance of the observed chains is always the same, they most likely all consist of the same atomic species. Under fortunate tip conditions the inner atomic structure of the chains could be imaged as displayed in Fig. 3. Obviously, they consist of *two* adjacent atomic rows with atoms directly opposing each other. Height profiles along and across the dual row structure as also given in Fig. 3 retrieve the atomic distances within the chains as well as its registry with respect to the substrate. The atomic distance along the

rows (profile I) is found to be  $2.6 \pm 0.2$  Å, which within the limits of errors coincides with the nearest neighbor distance in Ir (2.72 Å). The spacing between the two adatom rows is somewhat larger ( $3.3 \pm 0.2$  Å) and corresponds closely to the occupation of the hollow sites next to the center row of the troughs as indicated in the schematic model given in the inset of the STM image in Fig. 3. The small deviation from the hard sphere value (3.12 Å) might come from the fact that for adatoms the local symmetry of the sites is at best two-fold. The model proposed is further supported by profile II in Fig. 3, which indicates that the adatoms reside in the lowest position within the surface which is supposed to still be reconstructed. (Note that the dashed line in profile II is simply a continuation of the reconstruction profile in the left part.) Irrespective of the detailed structure of the island and of the region below it, it is evident that such an enhanced distance of the adatom rows could hardly arise on an unreconstructed surface. So, together with the fact that no defects of the surface reconstruction were observed outside the islands, it is evident that the early stages of Fe film growth proceed without any lifting of the substrate reconstruction.

With the biatomic chains consisting of Fe atoms only, there can be no place exchanges between Fe and Ir at that stage of Fe coverage. This is in line with low energy ion scattering (LEIS) studies by Tsong *et al.*<sup>33</sup> Atomic exchange was found only in case of the unreconstructed (1 $\times$ 1) surface. So, the present system behaves contrary to Fe/Au(100), where such processes have been shown to take place from the very beginning of Fe deposition.<sup>18</sup>

### C. Surface defects and island nucleation

Inspection of Fig. 2(b) tells that for room temperature and low coverage deposition the iron chain lengths typically amount to 50–200 Å with very small islands lacking. This indicates that even for a 0.07 ML Fe film the initial nucleation process was already completed at lower coverage and that the system is in the island growth regime. Along the reconstruction troughs the mutual distance of the islands is of the order of 1000 Å and the large majority of troughs imaged in Fig. 2(a) host only a single chain. In the perpendicular direction, however, there is apparently no correlation between chain locations. As already mentioned, this is indicative for long-range and one-dimensional diffusion of the Fe atoms at room temperature, with the one dimensionality obviously enforced by the corrugation of the reconstructed surface.

Further corroboration for the linear diffusion comes from the vicinity of surface defects. There, the distribution of Fe chains depends crucially on the orientation of the defect relative to the direction of the reconstruction troughs. This is best illustrated at the boundary between two perpendicular domains of the (5 $\times$ 1) reconstruction [Fig. 4(a)]. In the domain with the surface corrugation parallel to the boundary, the island distribution remains unchanged up to the very domain edge. In contrast, when the troughs end at the boundary, a strong accumulation of Fe atoms is observed there with a selvage width of the order of the typical length of Fe islands [ $\approx 200$  Å at 300 K, see Fig. 4(b)]. It is followed by a

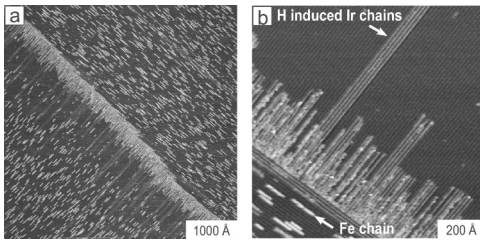


FIG. 4. (a) STM image ( $0.45 \times 0.45 \mu\text{m}$ ) containing the boundary between two orthogonal ( $5 \times 1$ ) reconstruction domains covered by 0.07 ML Fe grown at room temperature. (b) More detailed view of (a) ( $1000 \times 1000 \text{ \AA}$ ).

depletion zone which extends to several hundreds of  $\text{\AA}$  and contains practically no Fe. In the accumulation zone individual Fe chains cannot be resolved, instead atoms are agglomerated across the “hills” of the reconstruction. The atomic height within this coalesced regions is not uniform, but varies rather statistically. Obviously, the local atomic structure near the defect differs substantially from that of the Fe chains on the terraces. A discussion of this structure is postponed to Sec. IV.

The one-sided decoration of domain boundaries implies that the blocked ends of the troughs act as growth nucleation centers. This makes Fe atoms accumulate there while on plain terraces Fe islands are randomly distributed. Consequently, a depletion band must neighbor the accumulation in order to maintain the average atomic density of Fe. Other STM images show that also other defects like ascending and descending steps or islands effectively trap Fe atoms, as long as they block the troughs of the ( $5 \times 1$ ) reconstruction. When the distance between two of such defects falls below the diffusion length of Fe atoms (at room temperature in the range of  $1000 \text{ \AA}$ ), the depletion areas overlap leading to large uncovered areas.

Careful inspection of STM images such as that in Fig. 4(b) reveals an additional feature: There are also some darker (i.e., by about  $0.7 \text{ \AA}$  lower lying) but in most cases much longer lines which always start at surface defects. The density of these structures is directly correlated to both the ambient pressure and the time elapsed after preparation. They even develop on a formerly clean surface, though their appearance seems to be enhanced when Fe is present at the surface. In a forthcoming publication<sup>32</sup> such lines will be shown to be due to a local surface restructuring induced by adsorbed hydrogen whereby Ir rows are expelled from the hexagonal surface layer.

#### IV. LIFTING OF THE HEXAGONAL RECONSTRUCTION

##### A. Appearance in the STM

As demonstrated above, chainlike Fe islands can exist as a metastable phase on reconstructed Ir(100)-( $5 \times 1$ ) at room temperature or below. With two Fe atoms per ( $5 \times 1$ ) unit cell this phase might be expected to extend up to a total Fe coverage of 0.4 ML, provided it can spread homogeneously over the surface. Then an ordered array of one-dimensional atomic Fe wires would result, highly welcome for studies of

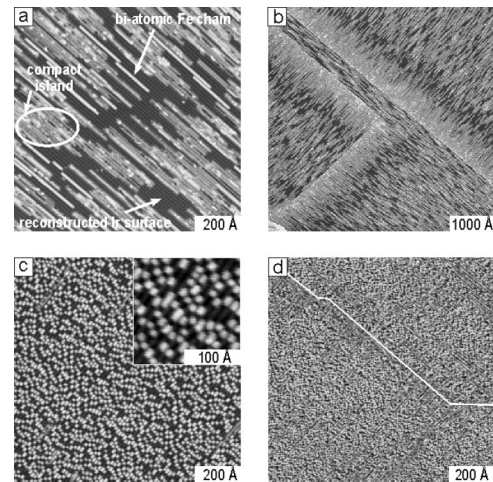


FIG. 5. STM images of a 0.25 ML Fe film deposited at about 300 K (a),(b) and 100 K (c),(d). (a) Image of a domain's center ( $1000 \times 1000 \text{ \AA}$ ) showing the coexistence of Fe chains, compact islands, and empty reconstructed regions. (b) Large scale image ( $0.5 \times 0.5 \mu\text{m}$ ) of domain boundaries. (c) More detailed view ( $1000 \times 1000 \text{ \AA}$ ) of a domain's center showing the homogeneous distribution of Fe chains on top of the reconstructed surface (see inset). (d) Large scale image ( $2000 \times 2000 \text{ \AA}$ ) of a domain boundary (marked by a white line).

magnetism in systems of reduced dimensionality. Yet, such a uniform phase cannot be prepared. Instead, for room temperature deposition the phase changes considerably when the iron coverage is increased to about 0.25 ML as demonstrated in Fig. 5(a). There are not only Fe chains (which now extend to a length of up to  $500 \text{ \AA}$ ) but also large compact islands indicating that growth is no longer confined to the troughs of the reconstruction [in addition, there are still extended regions completely uncovered by Fe and still exhibiting the clean surface ( $5 \times 1$ ) reconstruction]. The height of the compact islands as imaged in STM appears somewhat lower than for the Fe chains. The islands frequently appear streaky in accordance with the original periodicity of five (bulklike) unit meshes. At domain boundaries there is still some accumulation at one side followed by a (now less pronounced) depletion zone [Fig. 5(b)].

Interestingly, the STM appearance of the accumulation zones is very similar to that of the compact islands. The same holds for the defect accumulation zones observed at lower (global) coverage (Fig. 4) and for the long and already broadened islands developing upon high temperature Fe deposition [Fig. 2(c)] or upon annealing of low temperature deposited films. Therefore, we tentatively assign those regions to the same underlying structure. The geometry of the latter will be addressed in Secs. IV B and V. First, we discuss the fact that the island formation can be triggered by both annealing of a low coverage phase and a sufficiently high coverage. As the necessity of annealing proves the existence of an activation barrier, one might assume that the height of this barrier is coverage dependent. Yet, an alternative model might hold as discussed in the following.

The formation of compact islands prior to the completion of a homogeneous double-chain phase may be due rather to

kinetic than energetic reasons as plausible from the following consideration. At low coverage there is little chance that further deposited Fe atoms arrive at the unfavorable sites within a double chain. But even if so, they can easily diffuse to the end of the chain as the chains are still rather short. Yet, the probability for the occurrence of two long double-chains directly adjacent to each other—and so the chance of newly arriving Fe to impinge in between—increases quadratically with coverage. As the same holds for the diffusive random walk to one end of the chains (because chain nucleation is completed, the average chain length is proportional to coverage), the average residence of Fe atoms on the unfavorable sites increases dramatically and so the probability for the conversion into a locally more densely packed phase becomes suddenly competitive even in spite of a large activation barrier involved in this process. So, there is no need to postulate a coverage dependence of the activation energy to form the compact islands, though this cannot be ruled out. Regarding the further growth of the compact islands, STM images similar to that given in Fig. 5(a) tell that there is no local coexistence with the chain phase, i.e., compact islands and Fe chains are always well separated from each other. This means that once a dense nucleus has formed, all Fe available in the vicinity is completely incorporated in a kind of avalanche process. Equivalently, there is only a small activation energy (if ever) for growth of the dense phase.

As a consequence of the kinetic model proposed, a reduction of the average chain lengths should stabilize the metastable double-chain phase. This is indeed the case as deposition at low temperatures (100 K) but the same coverage (0.25 ML) shows [Fig. 5(c)]. The surface is now homogeneously covered by rather short Fe double chains residing in the troughs of the surface's reconstruction [see inset of Fig. 5(c)]. There are no indications for the formation of compact islands, not even next to domain boundaries [Fig. 5(d)], where only some hydrogen induced Ir lines are found. This is in spite of the intermediate warm up during sample transfer, i.e., without that the double-chain phase may be stabilized at even higher coverage. Nevertheless, with further Fe deposition the structural conversion proceeds quite rapidly in the range 0.30–0.35 ML prohibiting the formation of a homogeneous double-chain phase. The newly formed compact islands exhibit a rather streaky texture which is more pronounced than observed for room temperature deposition. The streaks align along the direction of the former reconstruction lines. However, there is no clear periodicity and no good atomic resolution could be achieved. Yet, it seems that locally detected straight lines are irregularly decorated by other material at most of their length. Both their unstructured appearance and apparent height largely resembles the Ir rows produced by hydrogen-induced restructuring of the surface [see Fig. 4(b)]. So, it appears plausible to predict a similar process induced by Fe and assign the newly formed islands to a certain joint arrangement of Ir and Fe atoms placed on an unreconstructed Ir(100) surface. Such a lifting of the surface reconstruction would also be in line with observations made by Andrieu *et al.*<sup>3,5</sup> for the growth of Fe/Ir superlattices. Also, it is a prerequisite of any pseudomorphic growth of bct iron on this surface.

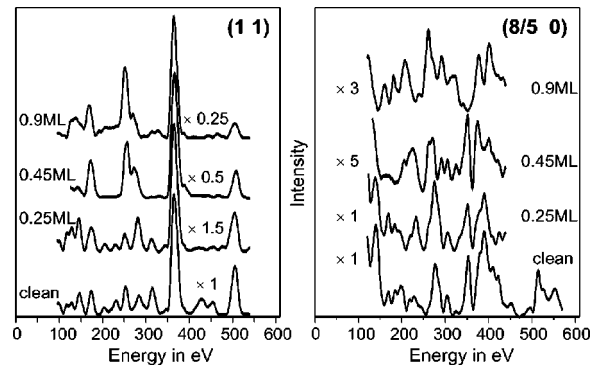


FIG. 6. Development of LEED  $I(E)$  spectra for one selected integer and fractional order beam (normalized in height) with Fe coverage evaporated at 100 K.

### B. Appearance in LEED

A better probe for the atomic structure of the compact islands is LEED, since its information depth extends a few layers below the islands and so provides sensitivity to a possible reconstruction of these layers. This is in particular true for Ir(100)-(5 $\times$ 1) as—because of the strong reconstruction involved—superstructure spots are exceptionally bright and even substrate spot intensities are considerably modified.<sup>16</sup> Therefore, LEED intensity spectra were taken for Fe deposition at 100 K for which the structural transition proceeds within a rather small and well defined coverage regime. Figure 6 compiles  $I(E)$  spectra for coverages just below and above the transition range (0.25 and 0.45 ML, respectively). For comparison, spectra for the clean and the (about) fully covered surface are displayed, too. Within the coverage regime 0–0.25 ML there are only minor changes of intensity spectra. This indicates that the scattering contributions of the Fe double chains arranged within the (5 $\times$ 1) reconstruction troughs and of the structural modifications induced are still small. This is in spite of the considerable scattering strength of Fe atoms and is due to the strong reconstruction of the surface which, though decaying in amplitude, extends to the fourth layer in the surface.<sup>16</sup>

The situation changes dramatically with further deposition of about 0.2 ML Fe inducing the structural transition. Average intensities of (fractional) integer order spots decrease (increase) considerably, so that their average ratio decreases by an order of magnitude. The increase of substrate spot intensities rules out that only some disordering takes place at the surface and allows to conclude that the new phase is structurally closer to a (1 $\times$ 1) arrangement of atoms. In view of sharp LEED patterns (not shown to save space) it must own long-range order, though—as indicated by some background and faint streaks—substantial short-range disorder must exist. The development of a new structure is also obvious from the drastic modifications of the spectral features of the intensities. In particular, the spectral changes in the fractional order data tell that the superstructure spots are not a residuum of the former hexagonal reconstruction. Instead, there is another kind of (5 $\times$ 1) structure. Its analysis will be the subject of Sec. V.

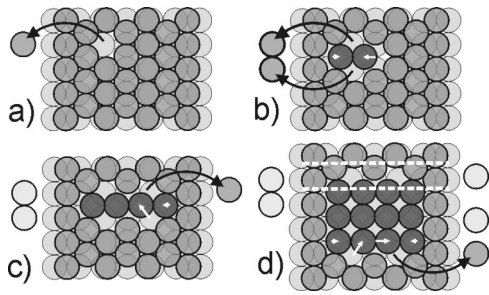


FIG. 7. Nucleation of  $(1 \times 1)$  ordered patches. The broken lines indicate one of the domain boundaries existing on both sides of the patches (for details see text).

### C. Model for the surface restructuring

The above observations are consistent with an iron induced surface restructuring in which the extra atoms in the hexagonal top layer are expelled to the surface where they arrange with the Fe atoms to form a new superstructure of (again)  $(5 \times 1)$  periodicity. The LEED intensities tell that the new superstructure is rather different from the former in accordance with the lifting of the (strong) hexagonal reconstruction. In a simple view, one just needs to extract one atom per  $(5 \times 1)$  unit cell in order to allow for the conversion from the hexagonally reconstructed surface into an unreconstructed, quadratic atomic arrangement. However, as revealed by Fig. 7(a), the removal of a single atom from the reconstructed layer gives only a little room for an atomic rearrangement (in a hard-sphere model only hopping of the created vacancy is allowed). For the creation of a  $(1 \times 1)$  ordered nucleus of minimum size the concerted removal of *at least two* atoms is required as indicated in Fig. 7(b). The resulting  $(1 \times 1)$  dimer can be easily doubled into a linear  $(1 \times 1)$  ordered quadruple just via the removal of a further atom [Fig. 7(c)]. Again this quadruple can be doubled (in direction normal to its extension) by removing only one more atom and each further removal of an atom allows for the formation of another quadruple [Fig. 7(d)]. Yet, additional to the request for the concerted removal of two atoms in the very beginning of the nucleation process two domain boundaries have to be formed along the two sides of the quadruple as indicated by broken lines in Fig. 7(d). Certainly, this formation is energy expensive so that for the whole nucleation process a considerably large activation energy must be expected, consistent with the activation necessary to trigger the structural transition within a large terrace. Once a  $(1 \times 1)$  patch has been nucleated, the surface restructuring proceeds in an avalanchelike process until all locally present Fe is consumed. Moreover, the above model also explains the reduced (if not negligible) activation connected with the transition starting at surface defects. There, the domain boundary already exists, so that the transition can simply spread.

## V. THE FORMATION OF AN ORDERED SURFACE ALLOY

As already mentioned, the new  $(5 \times 1)$  superstructure induced by Fe deposition is developed best in a coverage range

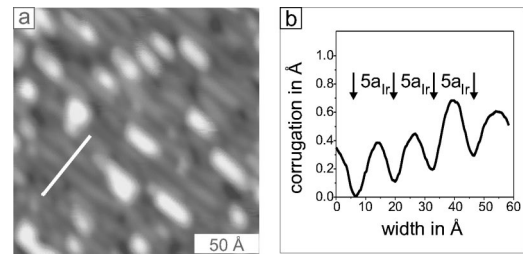


FIG. 8. (a) STM appearance of an Fe film near monolayer coverage (nominal: 0.9 ML) deposited at 100 K ( $200 \times 200 \text{ \AA}$ ). The height profile (b) is taken along the line indicated in (a).

of 0.8–0.9 ML Fe. The new top layer appears to be comparably flat, so that its atomic geometry should show up in the STM. This is investigated in the next subsection. The crystallography of this phase including deeper layers' structure can only be retrieved by quantitative LEED as demonstrated in the subsequent part.

### A. STM images

STM images for about monolayer Fe coverage deposited at room and low temperature appear to be rather homogeneous. An example for 0.9 ML Fe deposited at 100 K is displayed in Fig. 8(a), whereby the small bright patches represent the beginning of second layer growth. The height profile [Fig. 8(b)] reveals that the surface is linearly modulated with darker (i.e., by  $0.2 \text{ \AA}$  lower appearing) and almost equidistant lines equivalent to  $(5 \times 1)$  periodicity. From the apparent height as well as the density of these darker lines it is feasible to identify them with the linear rows of Ir atoms already found for lower coverage. This interpretation is also consistent with the findings of Gilarowski *et al.*<sup>17</sup> for Cu/Ir(100), where very similar lines had been unequivocally assigned to Ir by means of tunnelling spectroscopy. As a consequence, an ordered compound with  $\text{Fe}_4\text{Ir}$  stoichiometry has formed at around monolayer coverage as depicted schematically in Fig. 9(a). As the degree of order of the lines appears to be rather independent of the deposition temperature, the

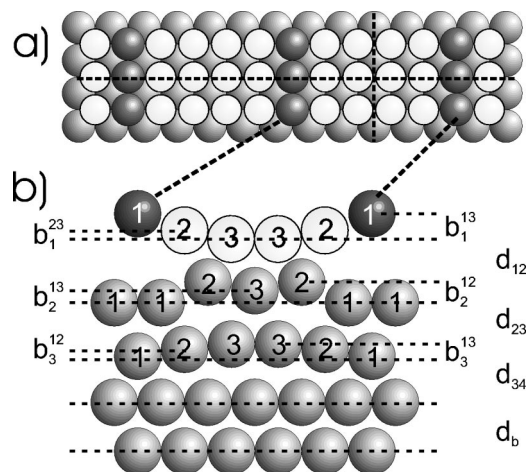


FIG. 9. Ball model for the  $\text{Fe}_4\text{Ir}$  compound on the Ir(100) surface in top (a) and side view (b). The latter also visualizes all structural parameters varied in the LEED analysis.

linear arrangement of Ir atoms within the compound layer seems to be produced already in the initial restructuring process, rather than by some long-range ordering interactions. The released atomic Ir rows are obviously immobile even at room temperature, so that Fe atoms just fill the space between them. Consequently, the ordered compound is not necessarily a stable configuration but might be kinetically stabilized.

### B. LEED structure determination

The model of a  $(5 \times 1)$  ordered surface compound easily explains the persistence of  $(5 \times 1)$  superstructure spots in LEED, even after the hexagonal reconstruction has been lifted by Fe. The gradual filling of the space between Ir rows by Fe is mirrored by the observed continuous modification of fractional order spectra with increasing coverage (Fig. 6). In order to corroborate and quantify this model a full-dynamical LEED intensity analysis was performed based on experimental data taken for a low temperature deposited film. With two orthogonal symmetry planes in the model [Fig. 9(a)] there are three symmetrically inequivalent atoms per  $(5 \times 1)$  unit mesh and layer. For each of them vertical coordinates were varied for the top three layers. From the result, we calculated average interlayer spacings  $d_{ij}$  (defined with respect to the center of mass planes of the layers) as well as intralayer buckling amplitudes  $b_i^{mn}$  between individual atoms  $m, n$  in layer  $i$  as defined in Fig. 9(b). All lateral coordinates were set to their bulk values, though shifts along the longer unit mesh vector are not forbidden by symmetry for most of the atoms. However, the atoms are rather densely packed laterally, leaving only little room for deviations from their ideal position. In order to simulate possible voids within the compound layer as imaged by STM, we additionally varied the concentration  $c_m$  of Fe atoms for the two sites  $m=2,3$  whereby, however, possible spatial correlations between vacancies were neglected. Also, contributions of atoms in the next deposited layer were neglected. Finally, vibrational amplitudes for first layer Fe and Ir atoms were varied independently as well as the amplitude common to all atoms below.

The resulting best fit is of good quality ( $R_P=0.22$ ), in particular in view of the size of the unit mesh and the enormous data base used which covers a total energy range  $\Delta E = 7753$  eV and  $\Delta E^{\text{int}} = 1909$  eV ( $\Delta E^{\text{frac}} = 5844$  eV) for the subsets of integer (fractional) order spots. The  $R$ -factors applying to these subsets ( $R_P^{\text{int}} = 0.13$ ;  $R_P^{\text{frac}} = 0.26$ ) tell that the bulk dominated integer order beam intensities are more accurately reproduced than the fractional order data. This might be due to the model approximations made or to some small residua of the former hexagonal reconstruction not detected in the STM. The visual comparison of experimental and best-fit calculated spectra (Fig. 10) demonstrates that the large majority of peaks in the spectra are reproduced, in most cases with the correct relative intensities. Given the broad data base this can be taken as a sound confirmation of the above model.

The structural parameters retrieved are compiled in Table I. The statistical error limits estimated through the variance of the  $R$  factor amount to about  $\pm 0.02$ – $0.03$  Å for the layer

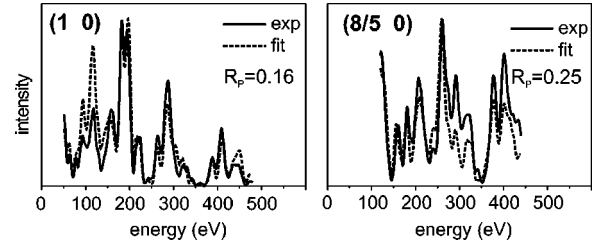


FIG. 10. Experimental and best-fit calculated LEED  $I(E)$  spectra for the  $\text{Fe}_4\text{Ir}$  surface compound on Ir(100) for two selected beams. The  $R$  factors given are single beam values.

spacings and bucklings, that for the Fe concentrations to about 10% of a monolayer. The comparably small errors result in spite of the only moderate  $R$ -factor level and come both by the large data base and the high electron energies (small wavelengths) applied as discussed in more detail elsewhere for the clean Ir(100) surface.<sup>16</sup> The best-fit model retrieved appears highly plausible: Fe atoms on both inequivalent sites are found at almost the same height, i.e., about 0.14 and 0.11 Å below the level of first layer Ir atoms. The second layer also shows a significant corrugation (0.08 Å) due to the bonding to chemically different neighbors within the overlayer. Atoms, which are exclusively coordinated to Fe atoms are lifted by 0.08 Å/0.06 Å relative to those located below the top layer Ir row. The corrugation proceeds also to the third layer, as expected with reduced total amplitude (0.04 Å) justifying the neglect of deeper layers' corrugation. The Fe concentrations in the top layer result as  $c_2 = 100\%$  and  $c_3 = 80\%$ , the latter value being consistent with the appearance of vacancies in the STM images. The vibrational amplitudes are 0.05 and 0.10 Å for top layer Ir and Fe atoms, respectively. The ratio of these values agrees with the amplitudes' scaling by the square root of the elemental mass. The amplitude of subsurface iridium atoms results as 0.05 Å consistent with the bulk Debye temperature of Ir (420 K).

The parameter values determined compare favorably with those retrieved for related structures. So, for clean Ir(100)- $(1 \times 1)$ ,<sup>16</sup> which results by just replacing the Fe atoms by Ir, the interlayer spacings  $d_{ij}$  are within 0.01 Å the same as in the present analysis (except for Fe atoms). Also, the bondlengths between Ir atoms located in the different buckled layers do not deviate by more than 0.04 Å from the corresponding values of the clean surface. These discrepancies might be even smaller in reality, since possible lateral atomic shifts were neglected in our analysis. Finally, the heterogeneous Fe-Ir bond lengths result to be 2.54, 2.55, 2.56, and 2.61 Å, i.e., close to the sum of atomic radii taken from bulk bcc-Fe and fcc-Ir (2.60 Å). Using the 1.6% contraction

TABLE I. Structural parameter values (in Å) determined for the  $\text{Fe}_4\text{Ir}$  surface compound on Ir(100) according to the model displayed in Fig. 9. The quantities  $d_{ik}$  correspond to the spacings between the center of mass planes of layers  $i, k$ .

$d_{12}$	$d_{23}$	$d_{34}$	$b_1^{13}$	$b_1^{23}$	$b_2^{12}$	$b_2^{13}$	$b_3^{12}$	$b_3^{13}$
1.74	1.95	1.92	0.14	0.03	0.08	0.06	0.03	0.04

of bond lengths calculated from the surface relaxation of bcc-Fe(100) (Ref. 34) and the corresponding value of 1.8% for fcc-Ir(100),<sup>16</sup> an interatomic distance of 2.55 Å would result, which fits even better to the above values. In total we can state that there are no unreasonable features in the structure of the ordered surface compound.

The structural analysis also reveals that top Ir atoms being imaged with STM by 0.2 Å lower than Fe atoms is a purely electronic effect since the real geometry is just the other way round. The surface compound is thus geometrically, chemically and electronically structured. For further film growth and provided the compound stays stable, it must be expected to act as an interface which imprints its periodic modulation into the growing film. Indeed, preliminary experiments with thicker Fe films unequivocally revealed a  $(5 \times 1)$  LEED pattern for 2 ML and even 5 ML thick Fe films grown at 100 K.<sup>35</sup>

## VI. CONCLUSION

Our investigations reveal that Fe deposited on Ir(100)- $(5 \times 1)$  destabilizes the hexagonal surface reconstruction with, however, a variety of kinetic limitations involved. So, on large plain terraces the activation barrier for surface restructuring must be rather high, since the nucleation of  $(1 \times 1)$  patches requires a concerted extraction of at least two atoms from the closed packed surface layer in order to establish the required light domain boundaries. Consequently, Fe deposited at low temperatures and with low coverage forms a metastable phase on the reconstructed surface with Fe double chains arranged in the troughs of the hexagonal overlayer. The chains grow in length with increasing coverage and temperature until at a certain value (which depends

on coverage and temperature) further growth is limited due to the large distances to be covered by surface diffusion. Then the occupation of unfavorable sites becomes competitive triggering the phase transition to the unreconstructed surface in an avalanchelike process. At surface defects, however, domain boundaries are already existent and therefore, the activation energy for restructuring is considerably reduced (if not negligible). Since the defects also act as effective traps for diffusing Fe atoms, they readily initiate the lifting of the reconstruction in their vicinity. Consequently, when the separation of defects is about 1000 Å on average, they dominate the initial growth behavior at the surface, at least for room temperature deposition.

Once the hexagonal reconstruction of the Ir(100) substrate is lifted, the atoms of the growing Fe film must arrange with the Ir atoms (0.2 ML) relieved from the former hexagonally reconstructed layer. The kinetics of the restructuring process leads to the development of linear atomic Ir rows aligned in direction of the former reconstruction troughs. These rows are practically immobile and form an ordered array in  $(5 \times 1)$  periodicity. The Fe atoms are accommodated between these rows which eventually leads to the formation of an ordered surface compound with  $\text{Fe}_4\text{Ir}$  stoichiometry. Such a patterned interface layer will certainly modify the further Fe growth on top of the compound and in this way the initial surface reconstruction of Ir(100) remains influential for even thicker films.

## ACKNOWLEDGMENTS

The authors are indebted to Deutsche Forschungsgemeinschaft (DFG) for financial support.

- 
- <sup>1</sup>V-L. Moruzzi, P.M. Marcus, and P.C. Pattnaik, *Phys. Rev. B* **37**, 8003 (1988).  
<sup>2</sup>V.L. Moruzzi, P.M. Marcus, and J. Kübler, *Phys. Rev. B* **39**, 6957 (1989).  
<sup>3</sup>S. Andrieu, M. Piecuch, L. Hennet, J. Hubsch, and E. Snoeck, *Europhys. Lett.* **26**, 189 (1994).  
<sup>4</sup>S. Andrieu, E. Snoeck, P. Arcade, and M. Piecuch, *J. Appl. Phys.* **77**, 1308 (1995).  
<sup>5</sup>S. Andrieu, F. L. Razafindramisa, E. Snoeck, H. Renevier, A. Barbara, J.M. Tonnerre, M. Brunel, and M. Piecuch, *Phys. Rev. B* **52**, 9938 (1995).  
<sup>6</sup>Ph. Bauer, S. Andrieu, O.M. Lemine, and M. Piecuch, *J. Magn. Magn. Mater.* **165**, 220 (1997).  
<sup>7</sup>M. Henkel, S. Andrieu, Ph. Bauer, and M. Piecuch, *Phys. Rev. Lett.* **80**, 4783 (1998).  
<sup>8</sup>D.C.A. Stoeffler, *J. Magn. Magn. Mater.* **198-199**, 306 (1999).  
<sup>9</sup>K. Louzazna and A. Haroun, *Thin Solid Films* **374**, 114 (2000).  
<sup>10</sup>S. Andrieu, C. Chatelain, M. Lemine, B. Berche, and Ph. Bauer, *Phys. Rev. Lett.* **86**, 3883 (2001).  
<sup>11</sup>A. Ignatiev, A.V. Jones, and T.N. Rhodin, *Surf. Sci.* **30**, 573 (1972).  
<sup>12</sup>E. Lang, K. Müller, K. Heinz, M.A. van Hove, R.J. Koestner, and G.A. Somorjai, *Surf. Sci.* **127**, 347 (1983).  
<sup>13</sup>W. Moritz (unpublished).  
<sup>14</sup>N. Bickel and K. Heinz, *Surf. Sci.* **163**, 435 (1985).  
<sup>15</sup>K. Johnson, Q. Ge, S. Titmuss, and D.A. King, *J. Chem. Phys.* **112**, 10 460 (2000).  
<sup>16</sup>A. Schmidt, W. Meier, L. Hammer, and K. Heinz, *J. Phys.: Condens. Matter* **14**, 12 353 (2002).  
<sup>17</sup>G. Gilarowski, J. Méndez, and H. Niehus, *Surf. Sci.* **448**, 290 (2000).  
<sup>18</sup>O.S. Hernán, A.L. Vásquez de Parga, J.M. Gallego, and R. Miranda, *Surf. Sci.* **415**, 106 (1998).  
<sup>19</sup>N. Spiridis and J. Korecki, *Appl. Surf. Sci.* **141**, 313 (1999).  
<sup>20</sup>N.W. Ashcroft and N.D. Mermin, *Solid State Physics* (Saunders College, Philadelphia, 1976).  
<sup>21</sup>V. Blum and K. Heinz, *Comput. Phys. Commun.* **134**, 393 (2001).  
<sup>22</sup>P.J. Rous, J.B. Pendry, D.K. Saldin, K. Heinz, K. Müller, and N. Bickel, *Phys. Rev. Lett.* **57**, 2951 (1986).  
<sup>23</sup>P.J. Rous, *Prog. Surf. Sci.* **39**, 3 (1992).  
<sup>24</sup>R. Döll, M. Kottcke, and K. Heinz, *Phys. Rev. B* **48**, 1973 (1993).  
<sup>25</sup>K. Heinz, R. Döll, and M. Kottcke, *Surf. Rev. Lett.* **3**, 1651 (1996).  
<sup>26</sup>U. Löffler, R. Döll, K. Heinz, and J.B. Pendry, *Surf. Sci.* **301**, 346 (1994).

- <sup>27</sup>J. Rundgren (unpublished).
- <sup>28</sup>Y. Gauthier, Y. Joly, R. Baudoing, and J. Rundgren, Phys. Rev. B **31**, 6216 (1985).
- <sup>29</sup>R. Baudoing, Y. Gauthier, M. Lundberg, and J. Rundgren, J. Phys. C **19**, 2825 (1986).
- <sup>30</sup>M. Kottcke and K. Heinz, Surf. Sci. **376**, 352 (1997).
- <sup>31</sup>J. Pendry, J. Phys. C **13**, 937 (1980).
- <sup>32</sup>L. Hammer, A. Schmidt, P. Landfried, W. Meier, and K. Heinz (unpublished).
- <sup>33</sup>T.T. Tsong, C. Chen, T.-Y. Fu, and Y.-R. Tzeng, Surf. Rev. Lett. **3**, 1259 (1996)
- <sup>34</sup>Z.Q. Wang, Y.S. Li, F. Jona, and P.M. Marcus, Solid State Commun. **61**, 623 (1987)
- <sup>35</sup>W. Meier, Ph.D. thesis, University Erlangen-Nürnberg, 2002.